Heliyon 11 (2025) e41500

Contents lists available at ScienceDirect

Heliyon

journal homepage: www.cell.com/heliyon

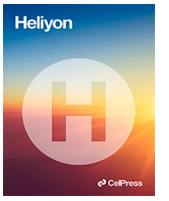

Research article

Abnormal dynamic features of cortical microstates for detecting early-stage Parkinson's disease by resting-state electroencephalography: Systematic analysis of the influence of eye condition

G. Gimenez-Aparisi [a], E. Guijarro-Estelles [a,e], A. Chornet-Lurbe [b], D. Cerveró-Albert [b], Dongmei Hao [c,d,e], Guangfei Li [c,d,e], Y. Ye-Lin [a,e,*]

[a] *Centro de Investigación e Innovación en Bioingeniería, Universitat Politècnica de València, 46022, València, Spain*
[b] *Servicio de Neurofisiología Clínica. Hospital Lluís Alcanyís, departamento de salud Xàtiva-Ontinyent, Xàtiva, 46800, València, Spain*
[c] *College of Chemistry and Life Science, Beijing University of Technology, 100124, Beijing, China*
[d] *Beijing International Science and Technology Cooperation Base for Intelligent Physiological Measurement and Clinical Transformation, 100124, Beijing, China*
[e] *BJUT-UPV Joint Research Laboratory in Biomedical Engineering, China*

ARTICLE INFO

Keywords:
Resting state electroencephalography
Parkinson
Microstate
Eyes influence
Dynamic features

ABSTRACT

Resting state electroencephalography (EEG) has proved useful in studying electrophysiological changes in neurodegenerative diseases. In many neuropathologies, microstate analysis of the eyes-closed (EC) scalp EEG is a robust and highly reproducible technique for assessing topological changes with high temporal resolution. However, scalp EEG microstate maps tend to underestimate the non-occipital or non-alpha-band networks, which can also be used to detect neuropathological changes. Recent evidence has shown that the source-space microstates can characterize distinct functional connectivity patterns but its clinical ability to detect neuropathological changes has not been demonstrated so far. It should also be remembered that the eye condition may play an important role in neural activity dynamics.

The aim of this study was to systematically characterize the dynamic neuropathological features of sensor-space and source-space EEG microstates in PD patients with no cognitive impairment in both EC and EO conditions with the aim of identifying potential biomarkers that could be used as a complementary clinical screening method for early PD detection. We found that the dynamic features of the source-space microstates were more sensitive in detecting PD than the sensor-space microstates, while EO was able to detect neuropathological changes in PD patients better than EC. In EO, PD disease exhibited significantly higher occurrence and coverage in visual-network related source-space microstates and abnormally high duration in sensorimotor network-related microstates. Our results suggest that the source-space microstate analysis of resting-state EEG could provide robust biomarkers to detect early-stage PD, which would allow the development of patient-oriented strategies to prevent the disease and improve the patients' quality of life.

* Corresponding author. Centro de Investigación e Innovación en Bioingeniería, Universitat Politècnica de València, 46022, València, Spain.
E-mail addresses: guigiap@ci2b.upv.es (G. Gimenez-Aparisi), eguijarro@ci2b.upv.es (E. Guijarro-Estelles), chornet_ant@gva.es (A. Chornet-Lurbe), marceralb@gva.es (D. Cerveró-Albert), haodongmei@bjut.edu.cn (D. Hao), guangfei.li@bjut.edu.cn (G. Li), yiye@ci2b.upv.es (Y. Ye-Lin).

https://doi.org/10.1016/j.heliyon.2024.e41500
Received 6 March 2024; Received in revised form 24 December 2024; Accepted 24 December 2024
Available online 26 December 2024

1. Introduction

Parkinson's disease (PD) is the second most common neurodegenerative disease, with a prevalence of 10 million worldwide [1,2]. It affects 1–2% of those over 60 years of age, with an increasing trend due to population ageing. Zhong et al. [3] estimated an increase of 155.51 % in the global Parkinson's disease between 1990 and 2019. PD is not only debilitating for the patient but is also one of the biggest social challenges with a huge economic burden on governments worldwide, including social security expenses, medication and loss of income, among others. The gross annual social economic burden was estimated at about $52 billion for approximately 1 million PD patients in the United States in 2017 [4]. Early detection is essential to help clinicians design a neuroprotective disease-modifying therapeutic program to prevent or slow down the progress of PD and provide patients with additional years of a better quality of life.

Neuropathological changes can precede the appearance of the clinical symptoms by up to a decade, giving rise to detectable abnormal neuronal activity [5]. However, diagnosis of PD in the prodromal stage is still restricted to the research field, although it will be important to design more effective therapies with a high repercussion on the patients' quality of life [6]. Increasing evidence has shown the effectiveness of resting state electroencephalography (EEG) for early PD detection [7–11]. Previous studies used different techniques for successfully extracting clinically meaningful biomarkers that correlate well with the severity of the disease, including the use of quantitative spectral analysis, functional connectivity analysis and non-linear dynamic analysis [12–17].

Microstate analysis describes broad-band spontaneous EEG activity in a limited number of scalp potential topographies (maps) that remain stable for a certain period of time (60–120 ms) but rapidly transition to a different topography that again remains stable [18]. Microstate analysis provides the topological changes in bioelectrical potential in milliseconds. Resting-state EEG microstates are robust and highly reproducible and are linked with functional magnetic resonance imaging (fMRI) resting-state networks [19]. Previous studies have identified the same four canonical EEG microstates (A, B, C, D) with high global explained topographical variance and appear to correlate with four well-known resting-state networks defined by fMRI [18,20]. Microstates with diagonal orientation (A and B), anterior-posterior (C) and fronto-central distribution (D) of the topographic map field have been consistently found in resting EEG, related to phonological processing, the visual network, the saliency network, and dorsal attention, respectively [20]. EEG microstate dynamics are modulated by different consciousness levels and diseases. Microstate analysis has been able to detect a variety of neurological disorders such as schizophrenia, anxiety disorders, autism, Alzheimer's disease, dementia, stroke, or multiple sclerosis, providing a reliable diagnosis and prognosis in easy-to-measure, task-free resting EEG recordings of only 3 min, which greatly contributes to transferring it to clinical settings [18].

Few previous studies have used microstate analysis to assess PD. Pal et al. [21] proposed scalp microstate from resting state EEG in the eyes closed (EC) condition to differentiate between cases of PD with and without dementia and healthy subjects. Chu et al. [22] found that dynamic scalp microstate features obtained from resting-state EEG in the EC condition could be used to differentiate between drug-free PD patients and healthy subjects. EEG microstates were also used to assess the effect of deep brain stimulation of the subthalamic nucleus [23]. Previous studies successfully reconstructed source microstate maps by projecting sensor-space microstates onto the surface of the cortex using brain source localization techniques [18,24]. However, this approach may still restrict our understanding of functional brain states due to several factors. Firstly, sensor-space EEG topographies have limited spatial resolution due to the blurring effect of volume conduction and so may not distinguish finer differences across maps. The sensor-space EEG microstate maps underestimate the importance of non-occipital or non-alpha-band networks, given the dominance of alpha-band occipital sources in the sensor-space eyes-closed resting-state EEG, which could be attributed to the shape of the head and the forward model [19,25]. Tait et al. [19] proposed a source-space microstate pipeline, obtaining 10 resting microstates with distinct functional connectivity patterns, although it is still unclear whether source-space microstates can detect neuropathology better than sensor-space microstates.

To the authors' knowledge, only two studies have to date assessed the usefulness of microstate analysis from scalp EEG in the EO condition in PD patients [26,27]. It is expected that visual processing during this condition could regulate the microstate dynamics. Indeed, it has been shown that microstate A had significantly shorter durations, while microstate C had increased occurrence [28] and microstate D had decreased coverage and duration in the EO condition [28]. Also, recent studies have shown that resting-state quantitative EEG in EO condition can better differentiate between PD and control subjects than EC [29–31] and no previous studies have assessed the ability of the EC and EO microstate dynamic features to detect PD neuropathology.

The aim of this study was thus to assess both the sensor-space and source-space EEG microstate dynamic features to differentiate between PD and healthy subjects in both EC and EO and also determine their relationship with clinical PD symptoms. This study is expected to provide the basic findings for the development of a simple quantitative real-time tool to promote EEG as a complementary screening technique for early PD detection in clinical practice, besides objectively monitoring the progress of the disease and/or

Table 1
Demographical information and clinical measurements from the database. The t statistic was used for continuous variables and the Chi-square for categorical variables.

	Control (N = 20)	PD (N = 13)	Test statistic	p-value
Sex (male/female)	8/12	6/7	0.05	0.82
Age, mean (SD)	68 (6.0)	68 (7.4)	−0.2	0.84
Disease duration, years, mean (SD)	n/a	5 (4.3)	n/a	n/a
Mini-mental state score, mean (SD)	28 (2.0)	28 (1.4)	−0.63	0.54
Beck's depression inventory, mean (SD)	5 (3.0)	8 (5.6)	−1.62	0.12
MDS-UPDRS, mean (SD)	5 (3.0)	29 (15.6)	−5.14	<0.001

evaluating the effectiveness of modifying therapies.

2. Materials and methods

2.1. Database

We used a public database consisting of 20 healthy subjects and 20 PD patients [32] but only performed the analysis for 13 of the PD patients who broke off their medication for 12 h before acquiring the data (medication OFF) to avoid any possible interference. Table 1 depicts the demographic and clinical information from the database. There were no significant differences in age, sex or the mini-mental state score between both groups. Beck's PD Depression score was slightly higher and with more variance, but not significantly, than in the healthy subjects. The PD patients showed a significantly higher MDS-Unified Parkinson's Disease Rating Scale (MDS-UPDRS) than the healthy subjects.

2.2. Signal preprocessing

The EEG signal was recorded by a 64-channel system with the NeuroOne Tesla amplifier. Two additional EOG channels were also recorded and the sample rate was 500 Hz. The raw data are available in Ref. [33]. Each register was compounded of a 2-min resting EEG with eyes closed, followed by another 2-minuterecording with eyes open. Preprocessing was by EEGLAB on Matlab. First, we applied a high-pass FIR filter by the Hamming window at 1 Hz to remove baseline fluctuations, followed by the FASTER toolbox in the default configuration (z-score$\geq$3) to automatically reject motion artifacts. Spherical interpolation was by adjacent channels. We split the continuous EEG into 2-s epoch data without overlap and used the FASTER toolbox to remove bad epochs (default configuration with z-score$\geq$3). We then applied independent component analysis (ICA) of the EEG epochs and inspected them visually to remove any remaining interference, such as cardiac, muscle and motion artifacts. We ended by projecting back to the original space to obtain the clean EEG epochs.

2.3. Microstate analysis

The microstate analysis was carried out in both the sensor-and source-space EEG in EC and EO using the +microstate toolbox [19]. We systematically compared the performance of two broad bandwidths commonly used in the literature for scalp-space and source-space microstate analysis: 2–20 Hz [22,27,34] and 1–30 Hz [19,25,35]. The scalp-recorded EEG was projected to cortical source-space EEG by the Exact Low Resolution Electromagnetic Tomography (eLORETA) [36] implemented in Fieldtrip (freely available at https://www.uzh.ch/keyinst/loreta.htm). ELORETA is a discrete, linear, 3D distributed imaging system that belongs to the weighted minimum norm inverse solution methods. It also has zero error localization, even with low spatial resolution. The solution space consists of 6239 voxels in the cortical grey matter at 5x5x5 mm^3 of spatial resolution in a realistic head model (standardised scalp-skull-brain head model) with MNI152 template [36]. Cortical parcellation was performed by computing the average power of all the voxels within each of 78 ROI, according to the AAL atlas [19].

The microstate analysis was conducted by a typical pipeline that consisted of identifying the global field power (GFP) peaks across the recordings, which are stable potential maps with the optimal signal-to-noise ratio. We randomly selected 5000 GFP peaks from each recording from all the healthy and PD subjects to group them into k global maps by a modified k-means clustering algorithm that uses the global map dissimilarity as the clustering criterion. For both sensor-space and source space EEG, we swept the number of global maps from 2 to 10 by the Kneedle algorithm to determine the optimum number of microstates.

After identifying the global maps from 165000 GFP peaks (5000 GEP peaks per subject x 33 subjects), we carried out the backfitting procedure to fully scan each GFP peak from each subject. All the GFP peaks in the whole dataset were labelled as a state based on the microstate centroid map with minimum distance. All the other samples were given the same state label as their nearest GFP peak. The following dynamic features were then computed for each subject.

- Duration: average duration of each microstate in milliseconds.
- Occurrence: average occurrences per second of the microstates.
- Coverage: percentage of the EEG covered by each microstate.
- Transition: probabilities of transitioning from one microstate to another.

2.4. Statistical analysis

We first conducted a Topographic Analysis of Variance (TANOVA) to assess the different topographies between the PD and healthy groups ($\alpha = 0.01$).

We carried out one-way ANOVA on the dynamic features of the microstates to assess the statistical differences between the PD and healthy subjects ($\alpha = 0.05$) for both EC and EO sensor-space and source-space data. We also computed Spearman's correlation between microstate dynamic features (duration, coverage occurrence and transition) and MDS-UPDRS ($\alpha = 0.05$). The FDR proposed by Benjamini-Hochberg corrections were used to minimize false positive in multiple comparisons for each microstate's state.

We also assessed significant differences in regional activation between PD and healthy subjects. Region activation shows the current density distribution of the parcellated cortical surface obtained through microstate analysis. It was first obtained by averaging

the current density distribution of each patient for the instants of each source-space microstate in both EC and EO. Statistical nonparametric mapping (available in LORETA-KEY software [37]) was then used to perform voxel-by-voxel independent F-ratio tests of the log-transformed current source density power between healthy and PD subjects ($\alpha = 0.05$). A nonparametric randomization procedure ($N = 5000$) was conducted to deal with multiple comparison and identify significantly different cortical voxels.

3. Results

3.1. Scalp and cortical microstates

Fig. 1 shows the EC and EO microstate maps obtained from the scalp EEG, in which the optimum cluster was 5. The four consistently found microstates in the resting state EEG were A and B with diagonal orientation, anterior-posterior C and D fronto-central, which have been linked to phonological, visual, the salience network and dorsal attention, respectively. We also identified the microstate F associated with the fronto-parietal network. We only found topographical differences between groups for EC microstate A and F ($p < 0.01$), while none were found in EO by the TANOVA analysis.

As depicted in Fig. 2, the optimum of the global maps of source state microstates was 5 and 7 for EC and EO, respectively. State 1 mainly reflect the visual network in EO, state 2 mostly represented left temporo-parietal and left sensorimotor activities, state 3 seems to be linked with right frontal, right frontal-temporal, and right sensorimotor activity, while state 4 is associated with left frontal activity in EC and EO. We also found right temporo-parietal-occipital activity in state 5, while state 5 in EO could be associated with bilateral frontal activities. States 6 and 7 in EO describes left frontal-parietal activities and bilateral sensorimotor activities, respectively. No topographical differences were found between PD and healthy groups in either EC or EO ($p > 0.01$).

3.2. Scalp and cortical microstate dynamic features

Table 2 shows the number of scalp and cortical microstate dynamic features that obtained the uncorrected p-value<0.05 to distinguish healthy subjects from PD for different bandwidths in both EC and EO, plus the significant correlations with MDS-UPDRS. The 2–20Hz bandwidth performed slightly better than the 1–30 Hz range for the scalp microstate. In the cortical microstates, the EC microstate dynamic features seemed to better discriminate PD and healthy subjects, although the correlation with MDS-UPDRS was higher in EO. In general, the scalp microstate dynamic features presented a poor discriminatory ability and correlation with MDS-UPDRS.

The dynamic features derived from the cortical microstate were noticeably better than those from the scalp in distinguishing PD and healthy subjects as well as their relationship with MDS-UPDRS. Unlike the scalp microstates, the 1–30 Hz bandwidth obtained slightly better results in source-space microstate analysis. As the EC microstate dynamic features seemed to better differentiate healthy and PD subjects, we only give the results of the cortical microstates.

Tables 3 and 4 give the results of the statistical analysis of the cortical microstate dynamic features in discriminating between healthy and PD subjects and their relationship with MDS-UPDRS in EC. We found a significantly lower coverage, occurrence frequency and duration in state 1, which was due to a reduced transition from states 2–5 to 1. The state 2 dynamic features remained almost stable, while only transition $4 \rightarrow 2$ decreased in PD subjects (uncorrected $p < 0.05$). The PD group had lower coverage of state 5 than healthy subjects (uncorrected $p < 0.05$), which was associated with the reduced transition of states $3 \rightarrow 5$ and $4 \rightarrow 5$. After FDR correction, no significant results were obtained for states 2 and 5. The PD subjects showed significantly higher coverage than healthy subjects, frequency of occurrence and duration of states 3 and 4, with a significant increase of transition from other states. Even after FDR corrections, the dynamic features obtained from states 1, 3 and 4 significantly differentiated the groups in EC.

In addition, the transitions of states $1 \rightarrow 1$, $2 \rightarrow 1$, $3 \rightarrow 1$, $4 \rightarrow 5$, $5 \rightarrow 5$ and the coverage and duration of states 1 and 5 presented a negative correlation with the MDS-UPDRS score with an uncorrected $p < 0.05$. The transitions of states $1 \rightarrow 4$, $2 \rightarrow 4$, $5 \rightarrow 3$, and $5 \rightarrow 4$ and the coverage and frequency of occurrence of state 4 was positively correlated with the MDS-UPDRS score with the uncorrected $p <$

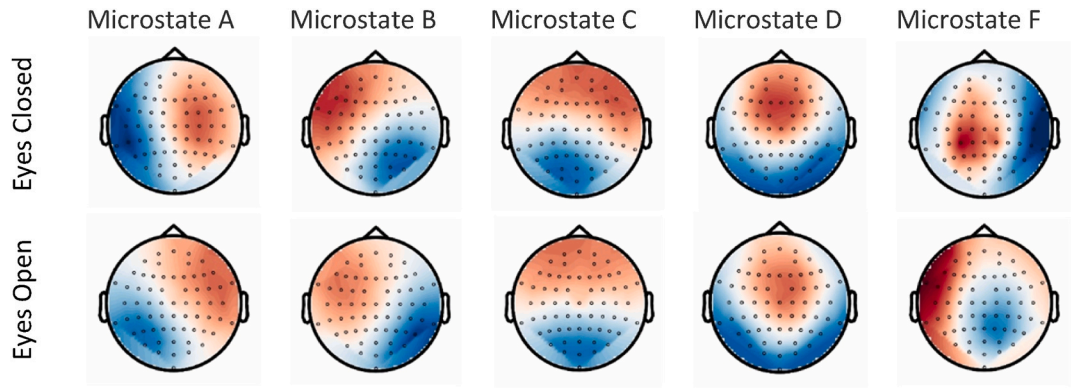

Fig. 1. Scalp microstates from resting state EEG in EC (Upper row) and EO (Lower row).

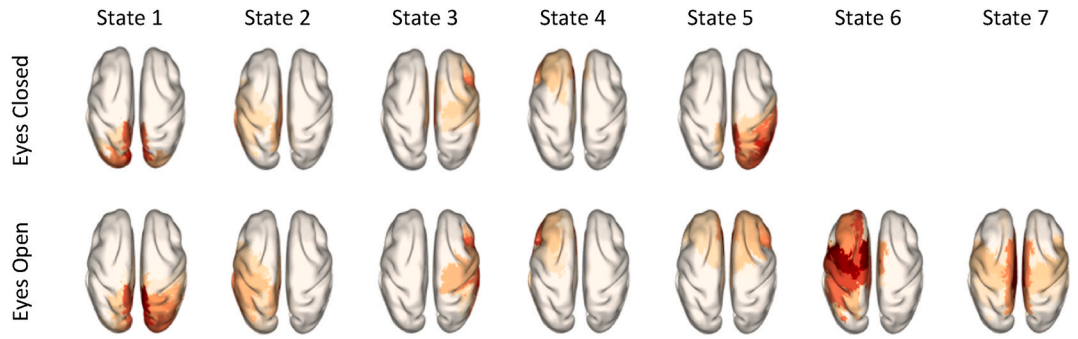

Fig. 2. Cortical microstate maps from resting state EEG in EC (Upper row) and EO (Lower row) after projection of EEG onto the cerebral cortex. A threshold of 60 % was applied. The optimum number of global maps (states) was 5 for EC, and 7 for EO.

Table 2
Number of dynamic features that obtained uncorrected p-value<0.05 to differentiate healthy and PD subjects and correlate with MDS-UPDRS for both EC and EO microstates derived from scalp and cortex.

		1–30 Hz		2–20 Hz	
		HC vs. PD	MDS-UPDRS	HC vs. PD	MDS-UPDRS
EC	Scalp	1	0	0	0
	Cortical	29	15	27	15
EO	Scalp	3	4	5	6
	Cortical	18	18	15	17

Table 3
Statistical analysis of dynamic cortical microstate features to distinguish healthy and PD subjects in EC. Increased and decreased features with uncorrected p-value<0.05 are shaded in blue and grey, respectively. Asterisk indicates statistically significant difference after FDR correction.

		To				
	HD vs. PD	State 1	State 2	State 3	State 4	State 5
Markov From	Duration	0.049*	0.437	0.007*	0.016*	0.081
	Coverage	0.007*	0.463	0.001*	0.006*	0.029
	Occurrence	0.010*	0.501	0.001*	0.006*	0.130
	State 1	0.009*	0.787	0.001*	0.030*	0.331
	State 2	0.007*	0.281	0.002*	0.016*	0.078
	State 3	0.013*	0.061	0.008*	0.027*	0.013
	State 4	0.020*	0.037	0.015*	0.025*	0.031
	State 5	0.017*	0.538	<0.001*	0.010*	0.154

Table 4
Spearman coefficient between MDS-UPDRS and dynamic cortical microstate features in EC. Positive and negative correlations with uncorrected p-value<0.05 are shaded in blue and grey, respectively. Asterisk indicates statistically significant difference after FDR correction.

		To				
	HD vs. PD	State 1	State 2	State 3	State 4	State 5
Markov From	Duration	-0.353	-0.211	0.305	0.216	-0.375
	Coverage	-0.432	-0.043	0.312	0.364	-0.362
	Occurrence	-0.302	-0.081	0.289	0.381	-0.297
	State 1	-0.353	0.096	0.327	0.362	-0.240
	State 2	-0.379	-0.211	0.260	0.437	-0.338
	State 3	-0.362	-0.254	0.307	0.232	-0.315
	State 4	-0.301	-0.235	0.182	0.216	-0.365
	State 5	-0.320	-0.028	0.418	0.431	-0.376

0.05, although after FDR correction no EC dynamic features significantly correlated with MDS-UPDRS.

Similar dynamic features were obtained for states 2 and 3 in EO, with no difference between both groups (see Table 5). Some dynamic features of states 4, 5 and 6 yielded weak differences between groups and/or weakly correlated with MDS-UPDRS (uncorrected $p < 0.05$), but with no significant results (see Table 6). The main changes in PD occurred for states 1 and 7; we found significantly higher coverage and frequency occurrence of state 1, with a significantly increased transition from states 2, 3, 5, 6, and 7 to 1 (FDR correction). These dynamic features, except the auto-transition of state $1 \rightarrow 1$, also showed a significantly negative correlation with MDS-UPDRS (FDR correction).

Both duration of state 7 and auto-transition $7 \rightarrow 7$ were significantly higher in the PD group, and also significantly correlated with MDS-UPDRS (FDR correction). Both coverage and transition of state $1 \rightarrow 7$ seemed to increase in the PD subjects, while the transition from state $2 \rightarrow 7$ was lower, but no significant result was achieved after FDR correction. Again, these dynamic features did not yield a significant positive correlation with the MDS-UPDRS score.

In the region activation difference between the groups we found similar results for different microstates under the same eye conditions. Table 7 shows the significant region activations between the healthy and PD group. In EC, PD showed hyperactivation in regions of the frontal lobe and also the anterior cingulate gyrus of the limbic lobe. The hypoactivation regions in PD were mostly located in the parietal lobe, along with regions in the limbic, temporal, and occipital lobes. The PD default mode network and the sensorimotor network showed hypoactivation.

We also found hyperactivation and hypoactivation in the frontal, and parietal lobes, but in different regions, except for the hyperactivation of the limbic lobe, which did not show any hypoactivation. These lobules were the frontal and parietal, including the hyperactivation of the left precentral gyrus (motor area) and the left postcentral gyrus (somatosensorial area), and the hypoactivation of the right postcentral gyrus (somatosensorial area). The interhemispheric asymmetry should be mentioned in EO, in contrast to EC, which had a more symmetric distribution. No significant activation was found for DMN in EO.

4. Discussion

4.1. Microstate dynamic features

This study involved a microstate analysis of both EC and EO sensor-space and source-space EEG. In a previous study, Pal et al. [21] considered the lower frequency of occurrence of microstate D to be the hallmark signature of PD in EC. The microstate of PD patients has also been shown to have longer durations and more frequent occurrence than in healthy controls in EC, but only the frequency of occurrence of microstate A significantly correlates with MDS-UPDRS [22]. Lamos [23] found that the time coverage of microstate D, associated with the supplementary motor area, reflected the effect of DBS treatment on PD motor symptoms, while the microstate of PD patients provided higher mean beta power than the control group. However, we did not find any difference in scalp microstate dynamic features between the PD and healthy groups in EC, which could be related to various factors. Firstly, our database was relatively small, which makes it more difficult to obtain statistical differences. The progressive nature of the disease, plus the additional confusion of a different disease etiology can also contribute to these controversial results [38]. In addition, we assessed the capability of scalp and source microstate dynamic features to predict PD in both EC and EO and confirmed that, although the scalp microstate features contained information to differentiate PD from healthy subjects, their performance was lower than the source space microstate features. We also confirmed the underperformance of EC in comparison to EO (the results are not shown in the manuscript due to the bias of the small sample size).

Serrano et al. [26] assessed the levodopa effect on PD using the resting state scalp microstate analysis in EO. They found that microstate A duration decreases after a levodopa intake and microstate B appears more times than before a levodopa intake, which

Table 5
Statistical analysis of cortical microstate dynamic features to distinguish healthy and PD subjects in EO. Significantly increased and decreased features (uncorrected p-value<0.05) are shaded in turquoise and grey, respectively. Asterisk indicates statistically significant difference after FDR correction.

		To						
	HC vs. PD	State 1	State 2	State 3	State 4	State 5	State 6	State 7
Markov From	Duration	0.458	0.539	0.917	0.090	0.047	0.092	0.006*
	Coverage	0.024*	0.321	0.148	0.047	0.101	0.111	0.024
	Occurrence	<0.001*	0.195	0.104	0.089	0.164	0.160	0.100
	State 1	0.164	0.153	0.290	0.068	0.138	0.187	0.047
	State 2	0.008*	0.490	0.091	0.030	0.296	0.126	0.037
	State 3	0.017*	0.505	0.867	0.109	0.109	0.179	0.079
	State 4	0.078	0.145	0.130	0.100	0.083	0.259	0.266
	State 5	0.004*	0.695	0.273	0.475	0.034	0.209	0.448
	State 6	0.009*	0.221	0.398	0.110	0.150	0.048	0.185
	State 7	0.010*	0.281	0.078	0.178	0.178	0.178	0.006*

Table 6
Spearman coefficient between MDS-UPDRS and cortical microstate dynamic features in EO. A significant positive and negative correlation (uncorrected p-value<0.05) is shaded in blue and grey, respectively. Asterisk indicates statistically significant difference after FDR correction.

		To						
	HD vs. PD	State 1	State 2	State 3	State 4	State 5	State 6	State 7
Markov From	Duration	-0.250	0.150	0.130	0.235	0.450*	0.370	0.499*
	Coverage	-0.502*	-0.132	-0.211	0.254	0.212	0.215	0.415
	Occurrence	-0.543*	-0.233	-0.284	0.211	0.151	0.186	0.300
	State 1	-0.250	-0.203	-0.153	0.222	0.215	0.179	0.408
	State 2	-0.553*	0.150	-0.260	0.282	0.148	0.184	0.275
	State 3	-0.536*	-0.165	0.130	0.231	0.143	0.233	0.251
	State 4	-0.477*	-0.213	-0.307	0.235	0.214	0.142	0.111
	State 5	-0.501*	-0.270	-0.174	0.121	0.450*	0.242	0.026
	State 6	-0.490*	-0.239	-0.173	0.212	0.168	0.370	0.206
	State 7	-0.564*	-0.085	-0.304	0.158	0.150	0.152	0.498*

could be due to lower fatigability in visual monitoring. Again, we did not find any significant alterations in these microstates. By contrast, we did find that microstate F in EO better differentiated PD patients and healthy subjects and better correlated with MDS-UPDRS (see Supplementary Material). The frontal-parietal network, which mainly occurs in 4–13 Hz α/θ rhythm, regulates the spontaneous decisions involved in planning and is essential for coordination in a rapid, accurate, and flexible goal-driven manner [39]. There is a great deal of evidence to show that PD is linked to the shifting of the dominant neuronal activity frequency from the alpha to theta rhythm, so that giving importance to the α/θ ratio may serve as one of the most typical characteristics of the disease [12,40,41].

To the author's knowledge, this is the first microstate analysis in source-space resting EEG to detect PD. We found that source-space microstate analysis is much more sensitive than sensor-space by carrying out a classification algorithm, but the number of subjects was not enough to generalise the results. The main changes were the higher duration of states 3 and 4, which are mainly linked to the right sensorimotor and left frontal activities. These changes could be related to alterations in the attention and executive functions present in PD [42–44]. We also found lower duration of state 1 focused on the occipital region in EC and a longer duration of the same state in EO, which is in line with recent studies that suggest reduced α-reactivity as a hallmark PD signature [45–48]. Physiologically, these phenomena reflect poor visual information processing in PD patients, which is associated with a marked deficit in the cholinergic system caused by degeneration of the nucleus basalis of Meynert [45]. Cholinergic dysfunction is also strongly linked to cognitive deficits in PD subjects with dementia [49]. A higher sensorimotor microstate duration has previously been associated with movement disorders [50] and cognition and perception functions [17], although no dynamic EC features showed a significant correlation with MDS-UPDRS after FDR correction. By contrast, the dynamic features of states 1, 5, and 7 in EO — associated with the visual network, bilateral frontal activities, and bilateral sensorimotor activities, respectively — showed a significant correlation with MDS-UPDRS, suggesting a relationship with clinical PD symptoms. In other words, the microstate dynamic features extracted from EO may better describe PD clinical symptoms than those obtained from EC. As this finding partially agrees with other studies [10,29–31] we therefore strongly recommend including EO in the clinical practice recording protocol.

4.2. Differences in region activation

The fact that we found significant activation regions between PD and healthy subjects in both EC and EO could be associated with the compensation mechanism for reorganizing resources in neurological disorders. Our EC results in general agree with previous fMRI studies. For example, Ma et al. [51] found that both tremor-dominant PD and postural instability-dominant PD contained disrupted regions that involved the basal ganglia, cerebellum, superior temporal gyrus, insula, pre- and postcentral gyri, inferior frontal gyrus, middle temporal gyrus, lingual gyrus, and parahippocampal gyrus, the last 5 of which match with our results. Pan et al. [52] showed that the most consistent and replicable findings in PD were hypoactivation in the bilateral supplementary motor areas, left premotor cortex, left inferior parietal gyrus, and hyperactivation in the right inferior parietal gyrus. This partially agrees with the hypoactivation in the bilateral inferior parietal lobule we found in the present work. The hypoactivity in the bilateral cuneus cortices were also replicable in 14 of the analysed datasets, which supports our results.

In comparison to healthy subjects, PD in normally cognitive patients showed significantly higher local neural synchronization in the right middle frontal gyrus and lower local synchronization in the left supramarginal gyrus, bilateral inferior parietal lobule, and the right postcentral gyrus [53]. PD subjects showed hypoactivity, default mode network (DMN), and in the sensorimotor network, [54–57]. This hypoactivation in the postcentral gyrus agrees with our result. Tessitore et al. [58] found reduced resting-state functional connectivity of the right medial temporal lobe and bilateral inferior parietal cortex in the DMN, which agree with our finding. We found PD subjects had hypoactivity in the bilateral inferior temporal gyrus extending to other regions of the DMN, such as the fusiform and parahippocampal gyri and precuneus, in line with previous studies [59,60].

Increased neuronal synchronization was found in PD patients in the frontal, primary sensory cortex, and cerebellar regions [55,56,

Table 7
Brain regions that yield an activation when comparing PD patients and healthy subjects. The regions in the first column are classified as hyper or hypo activated and EC or EO. Regions belonging to the DMN are shaded in green, and the sensorimotor network in orange.

Regions	Hyperactivation		Hypoactivation	
	EC	EO	EC	EO
Superior Frontal Gyrus, Frontal Lobe, BA9	X			
Medial Frontal Gyrus, Frontal Lobe, BA10	X			
Right Middle Frontal Gyrus, Frontal Lobe, BA 46				X
Middle Frontal Gyrus, Frontal Lobe, BA9	X			
Left Precentral Gyrus, Frontal Lobe, BA 6		X		
Left Inferior Frontal Gyrus, Frontal Lobe, BA47				X
Anterior Cingulate Gyrus, Limbic Lobe, BA24	X	X		
Posterior Cingulate, Limbic Lobe, BA31			X	
Parahippocampal Gyrus, Limbic Lobe, BA19			X	
Inferior Parietal Lobule, Parietal Lobe, BA40			X	
Precuneus, Parietal Lobe, BA7			X	
Supramarginal Gyrus, Parietal Lobe, BA40			X	
Right Supramarginal Gyrus, Parietal Lobe, BA40				X
Postcentral Gyrus, Parietal Lobe, BA1			X	
Left Postcentral Gyrus, Parietal Lobe, BA2		X		
Right Postcentral Gyrus, Parietal Lobe, BA2				X
Right Superior Parietal Lobule, Parietal Lobe, BA7				X
Angular Gyrus, Parietal Lobe, BA39			X	
Middle Temporal Gyrus, Temporal Lobe, BA37			X	
Inferior Temporal Gyrus, Temporal Lobe, BA20			X	
Cuneus, Occipital Lobe, BA19			X	
Fusiform Gyrus, Occipital Lobe, BA19			X	
Lingual Gyrus, Occipital Lobe, BA19			X	

61,62]. Hyperactivation in the posterior supplementary motor area, the anterior cingulate cortex and the primary sensorimotor cortices was suggested as a cortical motor reorganization in PD during a complex sequential motor task [63]. These findings supported the hyperactivation in both medial and superior frontal gyrus as well as the left precentral gyrus in PD patients in this work. We found that the alteration of regional activation was symmetrically distributed in EC, and more lateralized in EO. We did not find any statistical difference in DMN between PD and healthy subjects in EO, suggesting that this network depends on the eye condition. This may be related to the fact that the effective connectivity within the DMN improved in EO, which could be related to mood and emotional perception [35]. This phenomenon was also present in the visual network, but the sensorimotor network remained altered regardless of the recording condition. The alterations of regional activation indicate disease-related functional deficits secondary to degeneration of the dopaminergic neurons of the nigrostriatal system, so that further studies should be conducted to corroborate the regulation of the eye state.

To sum up, PD showed abnormal brain activity in multiple regions, including the frontal, limbic, parietal, temporal and occipital lobes, which could have been due to the neuropathological brain reorganizing its functional networks. The most important of these changes included hypoactivation of the default mode network and the altered EC sensorimotor network and visual network, while the alteration of the regional activation occurred symmetrically in EC but was asymmetrically distributed in EO.

4.3. Limitations of the study and future perspectives

This work is not exempt from limitations; firstly, the sample size was relatively small and further studies should be carried out to further corroborate the results. It also limits the design of a robust and generalisable PD prediction and detection model. The half-width of the confidence interval with only 13 PD subjects can be expected to be relatively high (approximately 0.23 for a sensitivity of 0.75, which means it can range from 0.52 to 0.98) and calls its real usefulness into question. At least 70 patients are required in even a balanced database to obtain a computer-assisted aid prediction system for preterm labour with a sensitivity range of [0.8–1] and specificity of [0.8–1]. In this regard, the technical and scientific community urgently needs a comprehensive database that includes the various causes of PD and serves as a platform that benchmarks diverse methods and identifies the most reliable EEG biomarkers of the disease's progress. We did not evaluate whether the microstate dynamic features provided complementary or redundant information to quantitative EEG analysis or other techniques. Future works should be directed towards the development of computer-assisted AI tools to predict the risk of PD even in the prodromal phase before the first symptoms appear and estimate its progress. In this context, a 10-year longitudinal study of the general population with an age range of 50–60 could offer valuable insights into neuropathological EEG changes and aid in preventing neurodegenerative diseases.

The microstate analysis method we used can only recognize less than 90 % of the EEG signals in each subject. In this regard, Chu et al. proposed an EEG microstate recognition framework based on deep neural networks that yielded recognition rates of from 90 % to 99 % [64]. These anti-artifact properties will considerably simplify the signal preprocessing step, enhance reproducibility and help to transfer the system to clinical practice.

5. Conclusions

In this study we found that the source-space microstate dynamic features were more sensitive in discriminating PD from healthy subjects and also correlated better with the MDS-UPDRS score than those in the sensor-space microstate. Both the visual and sensorimotor networks-related source-space microstates showed abnormal dynamic features in both EC and EO, the latter being more sensitive in detecting neuropathological changes in PD. PD showed a significantly higher occurrence and coverage of the microstates related to the visual network in EO, along with an abnormally prolonged duration of the microstates associated with the sensorimotor network. These abnormal dynamic patterns not only distinguish PD patients from healthy controls but are also moderately correlated with the MDS-UPDRS score, emphasising the importance of including both the EC and EO conditions in the recording protocol.

EEG microstate analysis is thus seen to be a robust and reproducible technique that could provide a reliable diagnosis in a very short time and could be used as a complementary screening technique for early detection of PD and/or better evaluation of the progress of the disease.

CRediT authorship contribution statement

G. Gimenez-Aparisi: Writing – review & editing, Writing – original draft, Visualization, Validation, Software, Methodology, Investigation, Formal analysis, Data curation, Conceptualization. **E. Guijarro-Estelles:** Writing – review & editing, Visualization, Validation, Supervision, Resources, Investigation, Funding acquisition, Formal analysis, Conceptualization. **A. Chornet-Lurbe:** Writing – review & editing, Visualization, Supervision, Resources, Project administration, Investigation, Funding acquisition, Conceptualization. **D. Cerveró-Albert:** Writing – review & editing, Visualization, Supervision, Investigation, Conceptualization. **Dongmei Hao:** Writing – review & editing, Visualization, Supervision, Software, Investigation, Formal analysis. **Guangfei Li:** Writing – review & editing, Visualization, Supervision, Software, Investigation, Formal analysis. **Y. Ye-Lin:** Writing – review & editing, Writing – original draft, Visualization, Validation, Supervision, Software, Resources, Project administration, Methodology, Investigation, Funding acquisition, Formal analysis, Conceptualization.

Data and code availability

Data included in the article is referenced in article.

Funding

This work was supported by the European Union – NextGenerationEU under the Investigo program (INVEST/2022/67) and Polisabio (Polisabio 2021/A04).

Funding for open access charge: CRUE-Universitat Politecnica de Valencia.for open acceunding for open accèè

Declaration of competing interest

The authors declare the following financial interests/personal relationships which may be considered as potential competing interests:G. Gimenez-Aparisi reports financial support was provided by European Union - NextGenerationUE. If there are other authors, they declare that they have no known competing financial interests or personal relationships that could have appeared to influence the work reported in this paper.

Appendix A. Supplementary data

Supplementary data to this article can be found online at https://doi.org/10.1016/j.heliyon.2024.e41500.

References

[1] L. Hirsch, N. Jette, A. Frolkis, T. Steeves, T. Pringsheim, The incidence of Parkinson's disease: a systematic review and meta-analysis, Neuroepidemiology 46 (4) (May 2016) 292–300, https://doi.org/10.1159/000445751.
[2] C. Marras, et al., Prevalence of Parkinson's disease across north America, NPJ Parkinsons Dis 4 (1) (Dec. 2018) 21, https://doi.org/10.1038/S41531-018-0058-0.
[3] Q.Q. Zhong, F. Zhu, Trends in prevalence cases and disability-adjusted life-years of Parkinson's disease: findings from the global burden of disease study 2019, Neuroepidemiology 56 (4) (2022) 261–270, https://doi.org/10.1159/000524208.
[4] W. Yang, et al., Current and projected future economic burden of Parkinson's disease in the U.S, NPJ Parkinsons Dis 6 (1) (Dec. 2020), https://doi.org/10.1038/S41531-020-0117-1.
[5] D.W. Dickson, Parkinson's disease and parkinsonism: neuropathology, Cold Spring Harb Perspect Med 2 (8) (Aug. 2012), https://doi.org/10.1101/cshperspect.a009258 a009258–a009258.
[6] E. Tolosa, A. Garrido, S.W. Scholz, W. Poewe, Challenges in the diagnosis of Parkinson's disease, Lancet Neurol. 20 (5) (May 2021) 385–397, https://doi.org/10.1016/S1474-4422(21)00030-2.
[7] C.X. Han, J. Wang, G.S. Yi, Y.Q. Che, Investigation of EEG abnormalities in the early stage of Parkinson's disease, Cogn Neurodyn 7 (4) (2013) 351–359, https://doi.org/10.1007/s11571-013-9247-z.
[8] G.S. Yi, J. Wang, B. Deng, X. Le Wei, Complexity of resting-state EEG activity in the patients with early-stage Parkinson's disease, Cogn Neurodyn 11 (2) (2017) 147–160, https://doi.org/10.1007/s11571-016-9415-z.
[9] W. Zhang, et al., Analysis of brain functional network based on EEG signals for early-stage Parkinson's disease detection, IEEE Access 10 (2022) 21347–21358, https://doi.org/10.1109/ACCESS.2022.3150561.
[10] G. Gimenez-Aparisi, E. Guijarro-Estelles, A. Chornet-Lurbe, S. Ballesta-Martinez, M. Pardo-Hernandez, Y. Ye-Lin, Early detection of Parkinson's disease: systematic analysis of the influence of the eyes on quantitative biomarkers in resting state electroencephalography, Heliyon 9 (2023) e00938, https://doi.org/10.1016/j.heliyon.2023.e20625, 2405–8440.
[11] S. Bhat, U.R. Acharya, Y. Hagiwara, N. Dadmehr, H. Adeli, Parkinson's disease: cause factors, measurable indicators, and early diagnosis, Comput. Biol. Med. 102 (Nov. 2018) 234–241, https://doi.org/10.1016/J.COMPBIOMED.2018.09.008.
[12] A. Jaramillo-Jimenez, et al., Resting-state EEG alpha/theta ratio related to neuropsychological test performance in Parkinson's Disease, Clin. Neurophysiol. 132 (3) (Mar. 2021) 756–764, https://doi.org/10.1016/j.clinph.2021.01.001.
[13] J.N. Caviness, et al., Differential spectral quantitative electroencephalography patterns between control and Parkinson's disease cohorts, Eur. J. Neurol. 23 (2) (2016) 387–392, https://doi.org/10.1111/ene.12878.
[14] J.N. Caviness, Pathophysiology of Parkinson's disease behavior-a view from the network, Parkinsonism Relat Disord 20 (1) (2014) 39–43.
[15] C.J. Stam, Nonlinear dynamical analysis of EEG and MEG: review of an emerging field, Clin. Neurophysiol. 116 (10) (Oct. 2005) 2266–2301, https://doi.org/10.1016/J.CLINPH.2005.06.011.
[16] K.T.E. Olde Dubbelink, et al., Disrupted brain network topology in Parkinson's disease: a longitudinal magnetoencephalography study, Brain 137 (1) (2014) 197–207, https://doi.org/10.1093/brain/awt316.
[17] Q. Wang, L. Meng, J. Pang, X. Zhu, D. Ming, Characterization of EEG data revealing relationships with cognitive and motor symptoms in Parkinson's disease: a systematic review, Front. Aging Neurosci. 12 (Nov. 2020) 373, https://doi.org/10.3389/FNAGI.2020.587396/BIBTEX.
[18] C.M. Michel, T. Koenig, EEG microstates as a tool for studying the temporal dynamics of whole-brain neuronal networks: a review, Neuroimage 180 (Oct. 2018) 577–593, https://doi.org/10.1016/J.NEUROIMAGE.2017.11.062.
[19] L. Tait, J. Zhang, MEG cortical microstates: spatiotemporal characteristics, dynamic functional connectivity and stimulus-evoked responses, Neuroimage 251 (May 2022) 119006, https://doi.org/10.1016/J.NEUROIMAGE.2022.119006.
[20] A. Khanna, A. Pascual-Leone, C.M. Michel, F. Farzan, Microstates in resting-state EEG: current status and future directions, Neurosci. Biobehav. Rev. 0 (Feb. 2015) 105, https://doi.org/10.1016/J.NEUBIOREV.2014.12.010.
[21] A. Pal, M. Behari, V. Goyal, R. Sharma, Study of EEG microstates in Parkinson's disease: a potential biomarker? Cogn Neurodyn 15 (3) (Jun. 2021) 463, https://doi.org/10.1007/S11571-020-09643-0.
[22] C. Chu, et al., Spatiotemporal EEG microstate analysis in drug-free patients with Parkinson's disease, Neuroimage Clin 25 (Jan) (2020), https://doi.org/10.1016/J.NICL.2019.102132.
[23] M. Lamoš, M. Bočková, S. Goldemundová, M. Baláž, J. Chrastina, I. Rektor, The effect of deep brain stimulation in Parkinson's disease reflected in EEG microstates, npj Parkinson's Disease 2023 9 (1) (Apr. 2023) 1–7, https://doi.org/10.1038/s41531-023-00508-x.

[24] A. Custo, D. Van De Ville, W.M. Wells, M.I. Tomescu, D. Brunet, C.M. Michel, Electroencephalographic resting-state networks: source localization of microstates, Brain Connect. 7 (10) (Dec. 2017) 671, https://doi.org/10.1089/BRAIN.2016.0476.
[25] C. Zhang, et al., The temporal dynamics of Large-Scale brain network changes in disorders of consciousness: a Microstate-Based study, CNS Neurosci. Ther. 29 (1) (Jan. 2023) 296, https://doi.org/10.1111/CNS.14003.
[26] J. Ignacio Serrano, et al., EEG microstates change in response to increase in dopaminergic stimulation in typical Parkinson's disease patients, Front. Neurosci. 12 (OCT) (Oct. 2018) 408568, https://doi.org/10.3389/FNINS.2018.00714/BIBTEX.
[27] T.D. de C. Costa, et al., Are the EEG microstates correlated with motor and non-motor parameters in patients with Parkinson's disease? Neurophysiol. Clin. 53 (1) (Feb. 2023) 102839 https://doi.org/10.1016/J.NEUCLI.2022.102839.
[28] B.A. Seitzman, M. Abell, S.C. Bartley, M.A. Erickson, A.R. Bolbecker, W.P. Hetrick, Cognitive manipulation of brain electric microstates, Neuroimage 146 (Feb. 2017) 533–543, https://doi.org/10.1016/J.NEUROIMAGE.2016.10.002.
[29] A.H. Meghdadi, M.S. Karic, C. Berka, EEG analytics: benefits and challenges of data driven EEG biomarkers for neurodegenerative diseases, Conf Proc IEEE Int Conf Syst Man Cybern 2019-Octob (2019) 1280–1285, https://doi.org/10.1109/SMC.2019.8914065.
[30] S.M. Keller, et al., Computational EEG in Personalized Medicine: A Study in Parkinson's Disease, 2018, pp. 1–6 [Online]. Available: http://arxiv.org/abs/1812.06594.
[31] I. Suuronen, A. Airola, T. Pahikkala, M. Murtojärvi, V. Kaasinen, H. Railo, Budget-based classification of Parkinson's disease from resting state EEG, IEEE J Biomed Health Inform 27 (8) (Aug. 2023) 3740–3747, https://doi.org/10.1109/JBHI.2023.3235040.
[32] H. Railo, N. Nokelainen, S. Savolainen, V. Kaasinen, Deficits in monitoring self-produced speech in Parkinson's disease, Clin. Neurophysiol. 131 (9) (Sep. 2020) 2140–2147, https://doi.org/10.1016/j.clinph.2020.05.038.
[33] H. Railo, "OSF | Parkinson's disease: Resting state EEG." Accessed: February. 3, 2023. [Online]. Available: https://osf.io/pehj9/.
[34] C. Chu, et al., Temporal and spatial variability of dynamic microstate brain network in early Parkinson's disease, npj Parkinson's Disease 2023 9 (1) (Apr. 2023) 1–12, https://doi.org/10.1038/s41531-023-00498-w.
[35] Y. Wang, et al., Open eyes increase neural oscillation and enhance effective brain connectivity of the default mode network: resting-state electroencephalogram research, Front. Neurosci. 16 (Apr) (2022), https://doi.org/10.3389/FNINS.2022.861247.
[36] R.D. Pascual-Marqui, "Discrete, 3D Distributed, Linear Imaging Methods of Electric Neuronal Activity. Part 1: Exact, Zero Error Localization,", Llinas, Oct. 2007 [Online]. Available: https://arxiv.org/abs/0710.3341v2. (Accessed 8 January 2024).
[37] LOW RESOLUTION BRAIN ELECTROMAGNETIC TOMOGRAPHY, LORETA, sLORETA, eLORETA, by R.D. Pascual-Marqui. https://www.uzh.ch/keyinst/loreta. (Accessed 29 January 2024).
[38] A. Fim Neto, et al., Subthalamic low beta bursts differ in Parkinson's disease phenotypes, Clin. Neurophysiol. 140 (Aug. 2022) 45–58, https://doi.org/10.1016/J.CLINPH.2022.05.013.
[39] S. Marek, N.U.F. Dosenbach, The frontoparietal network: function, electrophysiology, and importance of individual precision mapping, Dialogues Clin. Neurosci. 20 (2) (Jun. 2018) 133, https://doi.org/10.31887/DCNS.2018.20.2/SMAREK.
[40] K. Novak, B.A. Chase, J. Narayanan, P. Indic, K. Markopoulou, Quantitative electroencephalography as a biomarker for cognitive dysfunction in Parkinson's disease, Front. Aging Neurosci. 13 (January) (2022), https://doi.org/10.3389/fnagi.2021.804991.
[41] M. Moazami-Goudarzi, J. Sarnthein, L. Michels, R. Moukhtieva, D. Jeanmonod, Enhanced frontal low and high frequency power and synchronization in the resting EEG of parkinsonian patients, Neuroimage 41 (3) (2008) 985–997, https://doi.org/10.1016/j.neuroimage.2008.03.032.
[42] H. Bin Yoo, E.O.D. La Concha, D. De Ridder, B.A. Pickut, S. Vanneste, The functional alterations in top-down attention streams of Parkinson's disease measured by EEG, Scientific Reports 2018 8 (1) (Jul. 2018) 1–11, https://doi.org/10.1038/s41598-018-29036-y.
[43] B. Perfetti, et al., Attention modulation regulates both motor and non-motor performance: a high-density EEG study in Parkinson's disease, Arch. Ital. Biol. 148 (3) (2010) 279 [Online]. Available:/pmc/articles/PMC3071648/. (Accessed 23 January 2024).
[44] H. Teramoto, A. Morita, S. Ninomiya, T. Akimoto, H. Shiota, S. Kamei, Relation between resting state front-parietal EEG coherence and executive function in Parkinson's disease, BioMed Res. Int. 2016 (2016), https://doi.org/10.1155/2016/2845754.
[45] J. Schumacher, et al., EEG alpha reactivity and cholinergic system integrity in Lewy body dementia and Alzheimer's disease, Alzheimer's Res. Ther. 12 (1) (2020) 1–13, https://doi.org/10.1186/s13195-020-00613-6.
[46] J.L.W. Bosboom, et al., Resting state oscillatory brain dynamics in Parkinson's disease: an MEG study, Clin. Neurophysiol. 117 (11) (Nov. 2006) 2521–2531, https://doi.org/10.1016/J.CLINPH.2006.06.720.
[47] C. Babiloni, et al., Reactivity of posterior cortical electroencephalographic alpha rhythms during eyes opening in cognitively intact older adults and patients with dementia due to Alzheimer's and Lewy body diseases, Neurobiol. Aging 115 (2022) 88–108, https://doi.org/10.1016/j.neurobiolaging.2022.04.001.
[48] E.A. Barcelon, et al., Grand Total EEG score can differentiate Parkinson's disease from Parkinson-related disorders, Front. Neurol. 10 (APR) (2019) 1–11, https://doi.org/10.3389/fneur.2019.00398.
[49] D. Aarsland, I. Litvan, D. Salmon, D. Galasko, T. Wentzel-Larsen, J.P. Larsen, Performance on the dementia rating scale in Parkinson's disease with dementia and dementia with Lewy bodies: comparison with progressive supranuclear palsy and Alzheimer's disease, J. Neurol. Neurosurg. Psychiatry 74 (9) (Sep. 2003) 1215–1220, https://doi.org/10.1136/JNNP.74.9.1215.
[50] Z. Li, et al., Dysfunctional brain dynamics of Parkinson's disease and the effect of acute deep brain stimulation, Front. Neurosci. 15 (Jul. 2021) 697909, https://doi.org/10.3389/FNINS.2021.697909/BIBTEX.
[51] L.Y. Ma, X.D. Chen, Y. He, H.Z. Ma, T. Feng, Disrupted brain network hubs in subtype-specific Parkinson's disease, Eur. Neurol. 78 (3–4) (Sep. 2017) 200–209, https://doi.org/10.1159/000477902.
[52] P. Pan, Y. Zhang, Y. Liu, H. Zhang, D. Guan, Y. Xu, Abnormalities of regional brain function in Parkinson's disease: a meta-analysis of resting state functional magnetic resonance imaging studies, Sci. Rep. 7 (Jan) (2017), https://doi.org/10.1038/SREP40469.
[53] Y. Xing, et al., Regional neural activity changes in Parkinson's disease-associated mild cognitive impairment and cognitively normal patients, Neuropsychiatr Dis Treat 17 (2021) 2697–2706, https://doi.org/10.2147/NDT.S323127.
[54] P.L. Pan, H. Zhan, M.X. Xia, Y. Zhang, D.N. Guan, Y. Xu, Aberrant regional homogeneity in Parkinson's disease: a voxel-wise meta-analysis of resting-state functional magnetic resonance imaging studies, Neurosci. Biobehav. Rev. 72 (Jan. 2017) 223–231, https://doi.org/10.1016/J.NEUBIOREV.2016.11.018.
[55] W. Guo, et al., Brain activity alterations in patients with Parkinson's disease with cognitive impairment based on resting-state functional MRI, Neurosci. Lett. 747 (Mar. 2021) 135672, https://doi.org/10.1016/J.NEULET.2021.135672.
[56] D.L. Harrington, et al., Aberrant intrinsic activity and connectivity in cognitively normal Parkinson's disease, Front. Aging Neurosci. 9 (JUN) (Jun. 2017) 270261, https://doi.org/10.3389/FNAGI.2017.00197/BIBTEX.
[57] I.H. Choe, S. Yeo, K.C. Chung, S.H. Kim, S. Lim, Decreased and increased cerebral regional homogeneity in early Parkinson's disease, Brain Res. 1527 (Aug. 2013) 230–237, https://doi.org/10.1016/J.BRAINRES.2013.06.027.
[58] A. Tessitore, et al., Default-mode network connectivity in cognitively unimpaired patients with Parkinson disease, Neurology 79 (23) (Dec. 2012) 2226–2232, https://doi.org/10.1212/WNL.0B013E31827689D6.
[59] J.R. Andrews-Hanna, J.S. Reidler, J. Sepulcre, R. Poulin, R.L. Buckner, Functional-anatomic fractionation of the brain's default network, Neuron 65 (4) (Feb. 2010) 550–562, https://doi.org/10.1016/J.NEURON.2010.02.005.
[60] R.L. Buckner, J.R. Andrews-Hanna, D.L. Schacter, The brain's default network: anatomy, function, and relevance to disease, Ann. N. Y. Acad. Sci. 1124 (Mar. 2008) 1–38, https://doi.org/10.1196/ANNALS.1440.011.
[61] Y. Li, P. Liang, X. Jia, K. Li, Abnormal regional homogeneity in Parkinson's disease: a resting state fMRI study, Clin. Radiol. 71 (1) (Jan. 2016) e28–e34, https://doi.org/10.1016/J.CRAD.2015.10.006.

[62] M. ge Li, et al., Alterations of regional homogeneity in Parkinson's disease with mild cognitive impairment: a preliminary resting-state fMRI study, Neuroradiology 62 (3) (Mar. 2020) 327–334, https://doi.org/10.1007/S00234-019-02333-7.
[63] U. Sabatini, et al., Cortical motor reorganization in akinetic patients with Parkinson's disease: a functional MRI study, Brain 123 (2) (2000) 394–403, https://doi.org/10.1093/BRAIN/123.2.394.
[64] C. Chu, et al., An enhanced EEG microstate recognition framework based on deep neural networks: an application to Parkinson's disease, IEEE J Biomed Health Inform 27 (3) (Mar. 2023) 1307–1318, https://doi.org/10.1109/JBHI.2022.3232811.